Multi-Granularity Video Object Segmentation

Sangbeom Lim^{1*}, Seongchan Kim^{1*}, Seungjun An^{3*}, Seokju Cho², Paul Hongsuck Seo^{1†}, Seungryong Kim^{2†}

¹Korea University ²KAIST ³Samsung Electronics {limsbeom, 2020320120, phseo}@korea.ac.kr¹, {seokju.cho, seungryong.kim}@kaist.ac.kr², sjun.an@samsung.com³



Figure 1: Comparison of granularities of video segmentation datasets: Visualization of (top) MUG-VOS masks annotated by our data collection pipeline and ground-truth masks of Youtube-VOS (Xu et al. 2018), DAVIS (Pont-Tuset et al. 2017), and UVO (Wang et al. 2021) data and (bottom) MUG-VOS dataset. MUG-VOS masks include various types and granularities of objects, parts, stuff, and backgrounds, even those not covered by existing datasets.

Abstract

Current benchmarks for video segmentation are limited to annotating only salient objects (i.e., foreground instances). Despite their impressive architectural designs, previous works trained on these benchmarks have struggled to adapt to realworld scenarios. Thus, developing a new video segmentation dataset aimed at tracking multi-granularity segmentation target in the video scene is necessary. In this work, we aim to generate multi-granularity video segmentation dataset that is annotated for both salient and non-salient masks. To achieve this, we propose a large-scale, densely annotated multi-granularity video object segmentation (MUG-VOS) dataset that includes various types and granularities of mask annotations. We automatically collected a training set that assists in tracking both salient and non-salient objects, and we also curated a human-annotated test set for reliable evaluation. In addition, we present memory-based mask propagation model (MMPM), trained and evaluated on MUG-VOS dataset, which leads to the best performance among the existing video object segmentation methods and Segment SAMbased video segmentation methods. Project page is available at https://cvlab-kaist.github.io/MUG-VOS.

Introduction

Video segmentation has been one of fundamental tasks in computer vision, aimed at predicting and tracking the masks corresponding to specified targets in video data (Yang, Fan, and Xu 2019; Kim et al. 2020; Wang et al. 2021). Video segmentation showed great performance on identifying object and consistently tracking the object, however has shown poor performance on unknown class that has not trained on supervised stage. To develop a model capable of detecting and segmenting a wide range of categories, it is necessary to construct a larger dataset that includes as many classes as possible. However, this approach is cost-inefficient and challenging, making it difficult to create a model that can handle various types of object masks.

To alleviate this burden, several video segmentation tasks such as video object segmentation (VOS) (Caelles et al. 2017) or interactive video object segmentation (Benard and Gygli 2017) provide additional references for the target by giving segmentation mask at the first frame or giving iterative refinement to clarify it. Unfortunately, these tasks also

encounter performance degradation when they aim to segment non-salient objects, as they are only trained on specific targets, such as objects and stuff, according to the training dataset. Their utility in real-world applications often struggles in certain cases, such as interactive video editing and open-world video understanding, which require to return valid segmentation mask tracks for any given segmentation prompt.

Regardless of the model's architecture, segmenting anything in a video scene requires extensive data. SA-1B (Kirillov et al. 2023), an image segmentation dataset for the Segment Anything task, averages 100 masks per image. In contrast, most video segmentation datasets (Athar et al. 2023b) have far fewer mask tracks per video and rely on costly human annotation, which, while reliable, is resource-intensive.

In this work, we introduce Multi-Granularity Video Object Segmentation (MUG-VOS) dataset to extend the success of segment anything to the video domain. Our goal is to provide annotations of varying granularity for target masks, covering a range of objects, parts, and backgrounds. MUG-VOS fundamentally differs from previous video segmentation datasets (Xu et al. 2018; Pont-Tuset et al. 2017; Wang et al. 2021) by addressing limitations of traditional Video Instance Segmentation and Video Panoptic Segmentation, which often relies on a closed vocabulary, such as the 40 categories in YouTube-VIS (Yang, Fan, and Xu 2019) or the 124 classes in VIPSeg (Miao et al. 2022a). While Openvocab Video Segmentation (Wang et al. 2023) manages unlimited classes via natural language descriptions, it typically focuses on salient objects and often miss background elements or partial objects.

To build a large-scale video segmentation dataset capable of segmenting various targets, we utilized SAM, which can segment anything in images. We propose a SAM-based data collection pipeline that leverages a simple IoU-based tracking method to generate diverse training data. This resulted in a new dataset with 77k video clips and 47M masks, designed to train and evaluate segmentation and tracking at multiple granularities masks. MUG-VOS includes diverse mask tracks—salient, non-salient, and partial objects—enabling training and evaluation of models to predict previously unmanageable masks in video segmentation. Fig. 1 clearly shows the difference between the MUG-VOS dataset and existing video segmentation datasets.

On the other hand, recent attempts to adapt SAM for video segmentation (Zhou et al. 2024) have faced challenges by using SAM primarily as an image segmentation tool. For example, SAM-PT (Rajič et al. 2023) tracks points from the first frame to propagate masks, while DEVA (Cheng et al. 2023) uses SAM to generate candidate masks for each frame, while XMem (Cheng and Schwing 2022) propagates these masks by matching them with IoU.

SAM's strength lies in its ability to generate masks of varying granularity from prompts. If this capabilities extend to the video domain, it could be highly valuable for real-world applications like interactive video editing (Lee et al. 2023; Zhang et al. 2024; Lee, Cho, and Lee 2023) and generation, where traditional methods fall short.

We also propose a Memory-based Mask Propagation

Model (MMPM) as a baseline for MUG-VOS . For MMPM, we utilize the pre-trained SAM encoder to leverage the rich knowledge of SAM. Specifically, we introduce a memory module that can store information about target objects from previous outputs. This memory module allows the model to generate consistent segmentation mask tracks throughout the video. MMPM processes video frames sequentially while attending the memories that are relevant to the current frame. This module enables the SAM structure to be directly applied in the video domain. Additionally, we evaluate existing video segmentation methods and MMPM on MUG-VOS test dataset. MMPM shows best performance quantitatively and qualitatively on MUG-VOS dataset.

Related work

Video segmentation

The segmentation task stands out as one of the most extensively researched areas within the field of computer vision, encompassing various sub-tasks such as instance segmentation (Wu et al. 2023; Zhang et al. 2023b; Meinhardt et al. 2023), semantic segmentation (Hu et al. 2020; Wang, Wang, and Liu 2021; Liu et al. 2020), and panoptic segmentation (Li et al. 2022; Qiao et al. 2020; Athar et al. 2023a).

Video semantic segmentation focuses on segmenting the same semantic class referring to segmentation results on different frames. This method mainly focuses on improving the temporal consistency of segmented results. Video instance segmentation further challenges the complex problem of consistently identifying the same instance even on the deformation, blur, and existence of similar object classes. Video panoptic segmentation (Kim et al. 2020) further challenges to segment background stuff as previous methods have not been discovered.

Despite the remarkable performance achieved by these methods, they often struggle when confronted with unseen classes, limiting their applicability in real-world scenarios. To address this limitation, the concept of open-world segmentation (Xu et al. 2023; Liu et al. 2022) has been introduced. In this paradigm, models are designed to handle not only known classes that have been seen on the train but also unseen ones. For example, the BURST (Athar et al. 2023b) dataset contains 482 labels, which can be categorized into 78 seen classes and 404 unseen classes. Similarly, the UVO (Wang et al. 2021) dataset has been developed to facilitate open-world segmentation, aiming to build class-agnostic segmentation models. These approaches prioritize the ability to segment unseen classes, albeit often at the expense of overall performance. In contrast, our model is specifically engineered to segment any class based on given input conditions, without compromising performance or being restricted by class distinctions.

Segment anything

SAM (Kirillov et al. 2023) has emerged as a powerful solution for image segmentation tasks, demonstrating impressive performance. What sets SAM apart is its ability to interpret user input in various forms, including points, bounding boxes, and text. This ability to interpret any prompt for-

mat enables users to provide segmentation guidance through multiple modalities, enhancing the model's usability and flexibility. Another key strengths of SAM lies in its iterative training approach, facilitated by the utilization of SA-1B (Kirillov et al. 2023), a dataset containing various granularity of masks. Through this iterative process, SAM refines its segmentation capabilities, learning from the data in SA-1B and continuously improving its performance. This iterative training strategy plays a crucial role in enhancing SAM's effectiveness, allowing it to adapt to diverse inputs. As a result, SAM has proven to be a highly effective tool for a wide range of image segmentation applications, offering promising results and paving the way for further advancements in this field.

Segment anything in video domain

In recent years, a variety of approaches have emerged to extend SAM to the video level. For instance, Tracking Anything (Zhu et al. 2023; Cheng et al. 2023) and DEVA (Cheng et al. 2023) fused SAM at the image level and propagated masks to future frames using a video object segmentation model. SAM-PT (Rajič et al. 2023) adopted a different strategy by sampling points from the mask and leveraging a point tracking model to estimate their positions in future frames. These estimated points were then utilized to generate masks using SAM. Meanwhile, SAM-PD (Zhou et al. 2024) tackled video segmentation as a prompt denoising task. Their method involved spreading jittered and scaled bounding boxes and then selecting them based on semantic similarity. However, these prior works employ independent methods for propagating masks. This approach introduces noise that accumulates errors as the timestep increases. In contrast, our method takes an end-to-end approach to handle video segmentation, eliminating the need for additional steps and thus mitigating error accumulation over time.

Dataset

Existing video segmentation datasets (Xu et al. 2018; Pont-Tuset et al. 2017; Wang et al. 2021; Miao et al. 2022b; Athar et al. 2023b) typically focused on salient target objects that can be defined as specific classes. However, there currently exists no dataset for training or evaluating a diverse granularity of masks in video segmentation task.

Despite the numerous datasets for image-level segmentation, video-level segmentation datasets are scarce. Additionally, the lack of densely annotated masks in current video datasets hinders the adaptation of SAM on video segmentation. In order to train and evaluate MMPM, a large-scale video segmentation dataset is needed. To satisfy such conditions, Annotating a mask in a handcrafted way is accurate, but costs a lot. Therefore, we employ a semi-automatic data generation process involving minimal human annotators. To create a sufficiently large and diverse dataset, we developed a data collection pipeline to collect video segmentation data with varied granularity masks. Our data collection pipeline produces the segmentation data in a step-wise manner, ensuring both the quality and quantity of the masks.

Data collection pipeline

We propose a data collection pipeline designed to autonomously derive video segmentation data from preexisting video sources. Our data collection pipeline exploits SAM to generate dense masks for each frame and leverages an optical flow model to establish temporal connections between masks across consecutive frames, thereby generating pseudo-masks for video segmentation.

More specifically, for the given video $V=\{v_t|t\in[1,T]\}$, where v_t is t-th frame image, and T is the number of frames, target masks M_t^i are defined as those obtained from the initial frame using SAM through grid point prompts. Masks from subsequent frames that are temporally consistent to the masks from the initial frame, where i is the index of the track containing the target masks. Following the initial frame, prior to obtaining the target mask in the t-th frame, candidate masks potentially serving as the target mask are predicted.

To generate the candidate masks C_t^i , the points P_t^i are sampled from the target mask M_{t-1}^i . Subsequently, the points W_t^i are derived by warping the sampled points P_t^i into the t-th frame utilizing a flow map $F_{t-1 \to t}$ predicted by a flow model.

$$P_t^i = \text{sample}(M_{t-1}^i) \tag{1}$$

$$W_t^i = \text{warp}(P_t^i, F_{t-1 \to t}) \tag{2}$$

$$F_{t-1\to t} = \text{flow}(v_{t-1}, v_t) \tag{3}$$

The sample function denotes the process of randomly selecting point coordinates on the mask, while the warp function represents the warping of a point or a mask according to the flow map. The flow function refers to the estimation of a flow map between two adjacent frames. Candidate masks C^i_t in the t-th frame are derived by applying the point prompts acquired from the warped points W^i_t to SAM. The target mask M^i_{t-1} is further warped to the t-th frame via the flow map $F_{t-1 \to t}$ to obtain the warped mask \tilde{M}^i_{t-1} . Subsequently, the Intersection over Union (IoU) between the warped mask \tilde{M}^i_{t-1} and the candidate masks C^i_t are computed, with the candidate mask exhibiting the highest IoU being designated as the target mask M^i_t in the t-th frame.

$$C_t^i = SAM(v_t, W_t^i) \tag{4}$$

$$\tilde{M}_{t-1}^{i} = \text{warp}(M_{t-1}^{i}, F_{t-1 \to t})$$
 (5)

$$M_t^i = \arg\max_{C_t^i} \text{IoU}(\tilde{M}_{t-1}^i, C_t^i)$$
 (6)

Quality assurance. Fully automated processes can induce significant errors in the evaluation procedure. To prevent errors from accumulating in the automated process, human annotators were tasked with manually tracking and generating masks. For efficiency, annotators were instructed to accept or reject the mask tracks produced by the data collection pipeline. If an error occurred, the annotators refined the mask at the frame level using SAM. More details can be found in the appendix.

To ensure the quality of the mask tracks in the dataset, we adopted a verification process. As human annotators conduct

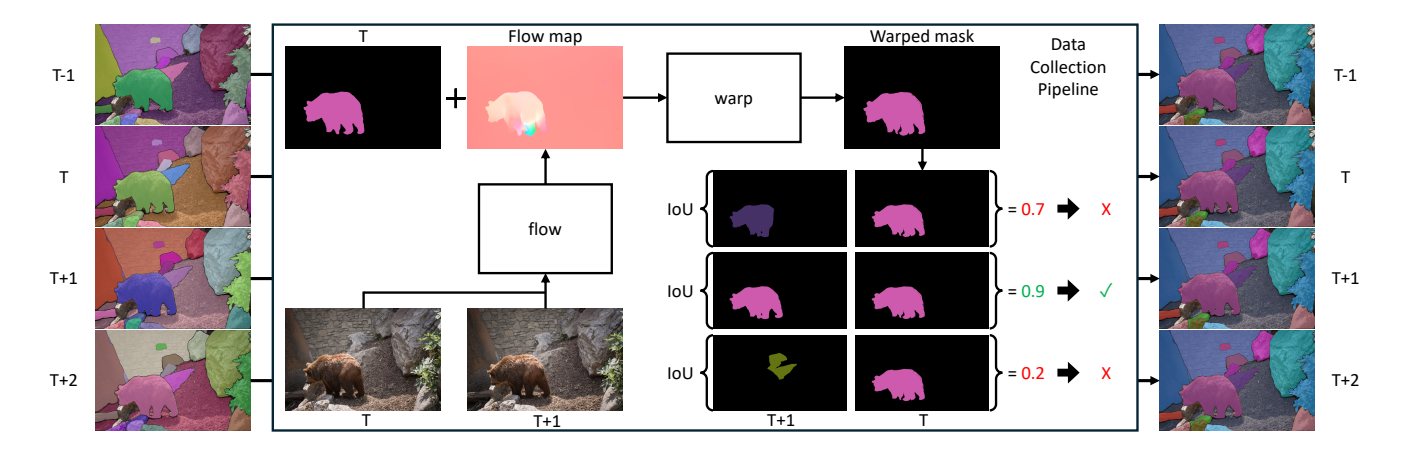


Figure 2: **MUG-VOS data collection pipeline.** We propose a data collection pipeline to generate a dataset to curate multigranularity mask tracks completely automatically. Using SAM, we generate a large number of masks per frame and find a temporal connection through the IoU between the mask warped from the previous frame and the mask from the current frame.

the tracking process, completed tracks are sent to a supervisor for approval. The supervisor reviews the annotated mask tracks alongside the original video to determine whether the tracks are satisfactory or unsatisfactory. Rejected mask tracks are sent back to the annotators for refinement. Quality assurance process was only done on the MUG-VOS test dataset.

MUG-VOS Dataset

The MUG-VOS dataset was built using our data collection pipeline and, to the best of our knowledge, is larger than any other video segmentation dataset.

Video collection. In the pursuit of crafting the video segmentation dataset, a judiciously selected subset of videos from the HD-VILA-100M (Xue et al. 2022) dataset was scrupulously curated for inclusion. The HD-VILA-100M dataset is devised to function as an expansive, high-resolution, and diversified video-language dataset, with the overarching goal of fostering multi-modal representation learning. This dataset encompasses a total of 3.3 M videos, characterized by their high caliber and equitable distribution across 15 categories. A subset of videos from this dataset was processed to get 77,994 video clips.

In addition, We create additional annotations for the 30 videos in the DAVIS-17(Pont-Tuset et al. 2017) validation set, which widely used in VOS task, for MUG-VOS test sets. We use SAM to generate average 29.6 mask tracks of varying types and granularities for each video.

Data generation. The MUG-VOS dataset facilitates training and evaluation on masks with various types and granularities, which are not covered by existing video segmentation datasets. Our data collection pipeline simplifies this process while ensuring high quality. To achieve this, we adapted our pipeline to the HD-VILA-100M and DAVIS-17 videos, resulting in a dataset that is both high quality and large in scale.

Data statistics. Table 1 presents the evaluation of related datasets and benchmarks for video segmentation. The density D of the segmentation masks is notated in Table 1 can

be given by the equation 7:

$$D = \frac{\sum_{i=1}^{H} \sum_{j=1}^{W} M_{i,j}}{H \times W}$$
 (7)

where as H is the height of the image, W is the width of the image, $M_{i,j}$ is the value of the mask at pixel (i,j), which is 1 if the pixel is covered by any mask and 0 otherwise.

For VOS tasks, common benchmarks include YouTube-VOS (Xu et al. 2018) and DAVIS (Pont-Tuset et al. 2017). Both datasets are annotated on in-the-wild videos, each lasting approximately 5-10 seconds. However, these datasets contain only a few mask tracks per video, which limits their ability to evaluate tracking performance across diverse masks.

The UVO (Wang et al. 2021) dataset primarily focuses on evaluating performance on unseen mask classes during training. It provides mask annotations for a variety of salient objects that humans typically recognize as "objects". While UVO covers a wide range of masks from a human perspective, it does not include non-salient objects that are not easily defined by humans, which remains as a limitation.

VIPSeg (Miao et al. 2022b) is part of the video panoptic segmentation benchmark. Video panoptic segmentation aims to predict the semantic class of every pixel in the temporal dimension. Compared to the datasets in Table 1, VIPSeg covers a higher density of pixels than any other dataset in Table 1. However, the masks in VIPSeg are much simpler compared to MUG, as the number of masks per frame is significantly lower than in MUG.

BURST (Athar et al. 2023b) is a universal dataset designed to cover multiple segmentation tasks, including video object segmentation, video instance segmentation, and point-guided segmentation (Guo et al. 2024; Zulfikar et al. 2024). While the aforementioned datasets primarily focus on annotating salient objects (e.g., humans, cars, animals), MUG-VOS includes a diverse range of class-agnostic masks.

Figure 3 shows visualization of our MUG-VOS test set.



Figure 3: **MUG-VOS test dataset.** To mitigate the accumulation of errors within the automated process, annotators were directed to either approve or reject the mask tracks generated by the data collection pipeline. In instances where errors were detected, the annotators performed frame-level refinements of the masks utilizing the Segment Anything Model (Kirillov et al. 2023).

	Density	Masks	Mask Tracks	Masks per Frame	Annotated Frames
OVIS (Qi et al. 2022)	0.186	296k	5,223	5.8	51,059
YT-VIS (Yang, Fan, and Xu 2019)	0.167	132K	4,866	1.69	79,260
YT-VOS (Xu et al. 2018)	0.184	17K	8,614	1.63	123,265
DAVIS (Pont-Tuset et al. 2017)	0.120	27K	386	2.6	150
UVO (Wang et al. 2021)	0.425	593K	104,898	12.3	58,140
BURST (Athar et al. 2023b)	0.167	600K	16,089	3.1	195,713
VIPSeg (Miao et al. 2022b)	0.979	926K	38,592	10.9	3,536
MUG-VOS Train	0.714	47M	4.7M	66.3	77,9940
MUG-VOS Test	0.663	59K	887	29.6	1,999

Table 1: **Data comparison with previous video segmentation datasets.** Comparing MUG-VOS with existing video segmentation datasets in terms of statistics.

Model

Figure 5 shows the overview of MMPM. For simplicity, the figure assumes a single object, but the MMPM model is designed to handle multiple objects simultaneously. MMPM consistently tracks objects and generates segmentation masks sequentially, frame-by-frame. Thanks to the memory module, which is designed to handle occlusion, motion blur, and deformation, the model can effectively track objects even in challenging video scenes. To build a robust video segmentation model, we incorporated two types of memory modules that function independently. For each frame, the RGB image is encoded by an image encoder, which serves as a query for the memory module. The encoded query from the image encoder accesses the memory bank to retrieve memory features that provide crucial information for generating the current mask. MMPM uses two types of memory: sequential memory and temporal memory, both of which are updated for selected frame. Frames selected for memory update are selected at regular intervals. Specifically, the temporal memory has a storage limit, T_{max} , to prevent running out of memory. When the temporal memory reaches a store limit, we randomly filter out memory entries, except for those from the first and previous frames. These memory features works as a enhancement for image feature to generate high-quality masks, even in long videos.

Temporal memory

The temporal memory stores information about previous predictions for the same target object in the video by maintaining high-resolution features for up to T_{max} recent frames. We split the memory into key and value components, which effectively retrieve relevant information. The key is encoded in the same embedding space as the query feature, while the value is encoded from a value encoder that fuses semantic and spatial information by encoding the image and binary mask together. Specifically, the key $\mathbb{R}^{C^k \times THW}$ exists in the same embedding space as the query feature, while the value is encoded independently.

For a selected frame, we copy the query feature from the image encoder as a key for the current frame. The generated key is then processed along with the binary mask from the mask decoder through the value encoder. The new key and

value from the current frame are then appended to the memory and provide important information for future decoding processes. When the number of temporal values reaches T_{max} , we randomly sample values, excluding those from the first and previous frames. The first frame's value provides initial information about the target object in the VOS task and is considered to best represent the target object. The value from the last frame contains the latest information about the target object.

This dynamic filtering of the temporal memory enables the model to represent both short-term and long-term object motion effectively.

Sequential memory

While temporal memory focuses on high-resolution features from previous frames, sequential memory focuses on low-resolution features such as geometric, semantic, and location information. Sequential memory complements temporal memory by updating the value on selected frame.

Specifically, sequential memory $S \in \mathbb{R}^{C^s \times HW}$ is updated every select frame using the query from the current frame. To effectively propagate sequential information, we use the GRU (Cho et al. 2014) method, which dynamically forgets previous information and updates with the current frame's information. The output from the value encoder serves as a candidate for updating the sequential memory. The GRU discards outdated information from the previous sequential memory and updates the sequential memory in parallel. This propagation process compensates for the lack of object information in temporal memory and stores new low-resolution information.

Experiments

Evaluation metric

For the evaluation metric, we use the Jaccard Index (\mathcal{J}) , the boundary F1-score (\mathcal{F}) , and the average of these metrics $(\mathcal{J}\&\mathcal{F})$ in the MUG-VOS dataset. In MUG-VOS, evaluation is performed independently for each individual mask, whereas in video object segmentation, evaluation is performed simultaneously across all masks in a frame.

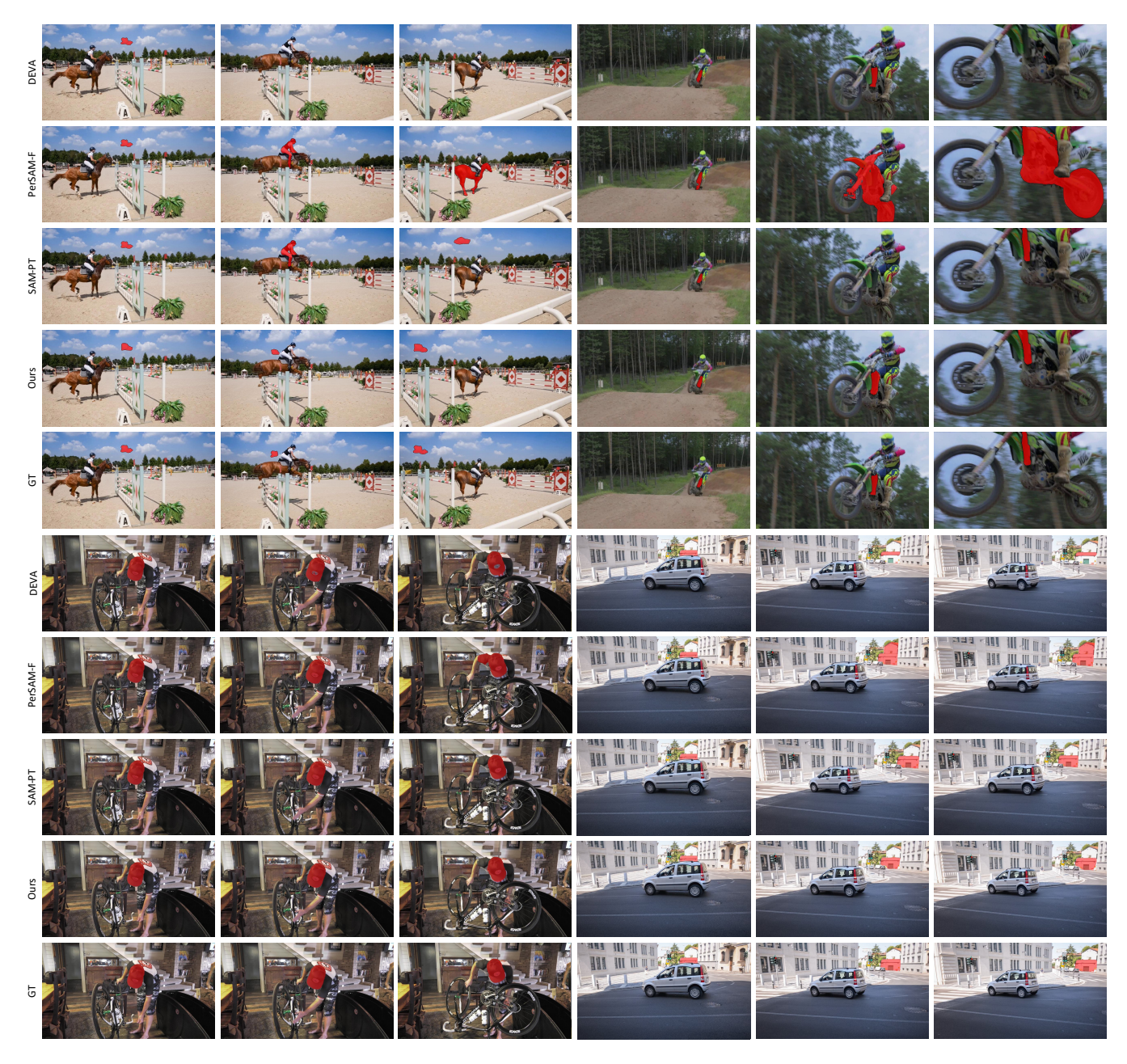


Figure 4: Qualitative comparison between MMPM, DEVA (Cheng et al. 2023), PerSAM-F (Zhang et al. 2023a), and SAM-PT (Rajič et al. 2023) from MUG-VOS test set.

MUG-VOS evaluation

In order to evaluate the capability of multi-granularity segmentation in a video scene, we tested our models on the MUG-VOS dataset, which contains high-quality masks with a variety of granularities. To demonstrate that our MMPM model is best suited to the MUG-VOS dataset, we also tested the MUG-VOS dataset with other existing models (Zhang et al. 2023a; Rajič et al. 2023; Cheng and Schwing 2022; Cheng et al. 2023). Specifically, since our MMPM leverages SAM's knowledge for video segmentation, we implemented a SAM-based baseline model that retrieves the mask proposal with the highest IoU score relative to the previous

frame. Masks were initialized by providing grid points to SAM on every frame, and mask tracks were subsequently generated by sequentially selecting the mask with the highest IoU score.

Table 2 shows the quantitative results on MUG-VOS dataset. For the SAM-based baseline, "Grid" refers to the number of points per side when sampling points from the grid. The baseline demonstrated poor performance because it fails to generate the current frame's mask without relying on prior information from the previous frame. Additionally, solely relying on IoU for track connection makes it vulnerable to significant motion changes and occlusions.

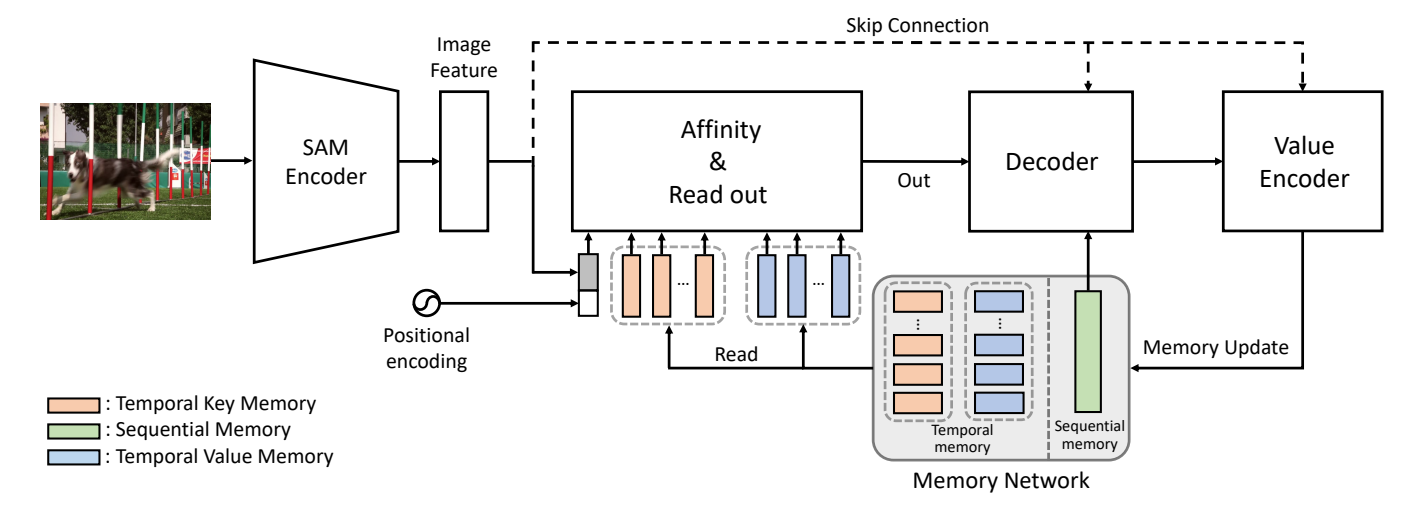


Figure 5: **MMPM overview.** We introduce the MMPM model, which generates masks based on previous results. Starting from an initial mask that indicates the target object, the MMPM model consistently tracks and segments the target throughout the entire video. Sequential memory stores low-resolution features, updated at every selected frames, while temporal memory retains high-resolution features from previous frames, capturing a variety of information gathered from multiple frames.

MUG-VOS Test	SAM	$\mathcal{J}\&\mathcal{F}$	${\cal J}$	${\cal F}$
zero-shot transfer				
SAM (Grid 32) + IoU	\checkmark	22.2	20.2	24.2
SAM (Grid 64) + IoU	✓	26.7	24.5	28.9
PerSAM (Zhang et al. 2023a)	✓	33.1	30.8	35.3
PerSAM-F (Zhang et al. 2023a)	✓	41.5	39.1	43.9
SAM-PT (Rajič et al. 2023)	✓	78.3	76.2	80.4
XMem (Cheng and Schwing 2022)	-	83.0	86.9	79.1
DEVA (Cheng et al. 2023)	-	85.6	<u>88.2</u>	82.9
MMPM	-	86.1	86.0	<u>86.1</u>

Table 2: The quantitative evaluation of video object segmentation on DAVIS-2017 (Pont-Tuset et al. 2017) validation set. Note that all the models are trained on the MUG-VOS train set. "SAM" correspond to an architecture that used SAM (Kirillov et al. 2023) Encoder and Decoder.

While XMem and DEVA have shown great performance on the VOS task, they performed poorly on the MUG-VOS test set. Our experiments not only demonstrate that the MMPM model achieved the highest score compared to other models but also highlight that the MUG-VOS dataset is more challenging compared to existing VOS benchmarks. Previous VOS benchmarks only evaluate performance on salient objects, allowing models to be tuned to find the most prominent objects. However, to be effective in real-world settings, models should be capable of segmenting diverse object regardless of the spatial position of the target.

Figure 4 shows the qualitative results compared with other methods. We will also provide more qualitative results in the appendix. MMPM demonstrated superior performance both quantitatively and qualitatively. We show more qualitative results on the Appendix E

Ablation study

We conducted ablation studies on the MMPM model using the MUG-VOS test dataset. These studies explore the effects

Methods	$\int \& \mathcal{F}$	$\mathcal J$	${\mathcal F}$
Not filter	85.0	85.7	84.2
FIFO	85.9	85.8	85.9
Random	86.0	85.9	86.0
+ P. first & last	86.1	86.0	86.1

Table 3: Ablation studies on memory filtering methods.

of different memory filtering methods, the number of memory values, memory update intervals, and the characteristics of each memory module.

Table 3 shows the performance of the MMPM model with different memory filtering methods. Firstly, no filtering is applied (i.e. Not filter) when memory reaches the limit T_{max} and the memory retains the first inserted values for the entire video. Secondly, to append the latest values to memory, we implemented the First-In-First-Out (FIFO) method. Performance gain from FIFO method enables MMPM model to generate segmentation masks with the latest information

Methods	J&F	\mathcal{J}	\mathcal{F}
No memory	81.8	85.3	78.2
+ Only sequential	81.9	85.3	78.5
+ Only temporal	85.7	85.9	85.8
+ Both	86.1	86.0	86.1

Table 4: Ablation studies on types of memory usage.

r	$\mathcal{J}\&\mathcal{F}$	$\mathcal J$	\mathcal{F}
1	66.6	50.4	82.8
3	68.3	52.2	84.4
5	86.1	86.0	86.1

Table 5: Ablation studies on memory update interval.

enables the model to find corresponding objects efficiently. Thirdly, randomly filtering values from the memory allows the model to access diverse memories with random interval. Lastly, applying a constraint to the random filtering method to preserve the first and last frame values (i.e. P. first & last), enhanced model performance compared to any other methods. Since, in VOS tasks, the initial mask from the first frame best represents the target object, and providing the latest mask to the MMPM model has a similar effect to the initial mask.

Table 4 shows the performance comparison between different memory usage types. To demonstrate the advantage of memory usage, we experimented with the MMPM model without memory values, where the mask is generated by referring only to the previous mask, indicated as 'No memory'. Adding sequential memory, which is updated from selected frame, improved performance. The low-resolution sequential memory helps the model retrieve the target object. When temporal memory is added, the high-resolution information further enhances the model's ability to segment high-quality masks, as temporal memory stores diverse target information (e.g., shape, color, motion) from multiple frames.

Table 5 shows the performance variation based on the interval period, denoted as r, which determines when to update the memory. Increasing the interval between memory updates allows the model to perform faster inference while enabling it to store diverse information in memory. This also demonstrates that our model is robust enough to handle significant appearance changes while effectively mitigating drifting and error accumulation (Oh et al. 2019; Yang, Wei, and Yang 2021). However, selecting an interval value that is too high can result in the loss of important intermediate information.

Table 6 shows the performance variation when implementing different number of memory values in the temporal memory, denoted as *N*. Increasing number of value stored in temporal memory gave MMPM model to look over various memories. Abundant information from past frames enabled model to enhance to image embedding, resulting to MMPM to generate high quality segmentation mask (Duke et al. 2021). Interestingly, MMPM model performance has converged around the number of values 10.

N	$\mathcal{J}\&\mathcal{F}$	\mathcal{J}	\mathcal{F}
5	85.7	85.8	85.5
10	86.1	86.0	86.1
15	86.1	86.0	86.1

Table 6: Ablation studies on number of temporal memory values.

Conclusion

In this work, we introduce the MUG-VOS dataset, designed for training and evaluating multi-granularity masks in the video domain. To create this dataset, we developed a data collection pipeline that constructs a large-scale, densely annotated video segmentation dataset, resulting in MUG-VOS. Our dataset includes diverse segmentation masks that are not limited to salient objects but also cover non-salient objects. We also present a video segmentation model named MMPM, which demonstrates superior performance compared to existing models on the MUG-VOS test dataset. We anticipate that the MUG-VOS benchmark will serve as a valuable resource for training and evaluating multi-granularity masks.

References

Athar, A.; Hermans, A.; Luiten, J.; Ramanan, D.; and Leibe, B. 2023a. TarViS: A Unified Architecture for Target-based Video Segmentation. In *CVPR*.

Athar, A.; Luiten, J.; Voigtlaender, P.; Khurana, T.; Dave, A.; Leibe, B.; and Ramanan, D. 2023b. Burst: A benchmark for unifying object recognition, segmentation and tracking in video. In *Proceedings of the IEEE/CVF winter conference on applications of computer vision*, 1674–1683.

Benard, A.; and Gygli, M. 2017. Interactive video object segmentation in the wild. arXiv preprint arXiv:1801.00269.

Caelles, S.; Maninis, K.-K.; Pont-Tuset, J.; Leal-Taixé, L.; Cremers, D.; and Van Gool, L. 2017. One-shot video object segmentation. In *Proceedings of the IEEE conference on computer vision and pattern recognition*, 221–230.

Cheng, H. K.; Oh, S. W.; Price, B.; Schwing, A.; and Lee, J.-Y. 2023. Tracking anything with decoupled video segmentation. In *Proceedings of the IEEE/CVF International Conference on Computer Vision*, 1316–1326.

Cheng, H. K.; and Schwing, A. G. 2022. Xmem: Long-term video object segmentation with an atkinson-shiffrin memory model. In *European Conference on Computer Vision*, 640–658. Springer.

Cheng, H. K.; Tai, Y.-W.; and Tang, C.-K. 2021. Rethinking space-time networks with improved memory coverage for efficient video object segmentation. *Advances in Neural Information Processing Systems*, 34: 11781–11794.

Cho, K.; Van Merriënboer, B.; Bahdanau, D.; and Bengio, Y. 2014. On the properties of neural machine translation: Encoder-decoder approaches. *arXiv preprint arXiv:1409.1259*.

- Duke, B.; Ahmed, A.; Wolf, C.; Aarabi, P.; and Taylor, G. W. 2021. Sstvos: Sparse spatiotemporal transformers for video object segmentation. In *Proceedings of the IEEE/CVF conference on computer vision and pattern recognition*, 5912–5921.
- Guo, D.; Fan, D.-P.; Lu, T.; Sakaridis, C.; and Van Gool, L. 2024. Vanishing-Point-Guided Video Semantic Segmentation of Driving Scenes. *arXiv* preprint arXiv:2401.15261.
- Hu, P.; Caba, F.; Wang, O.; Lin, Z.; Sclaroff, S.; and Perazzi, F. 2020. Temporally distributed networks for fast video semantic segmentation. In *Proceedings of the IEEE/CVF Conference on Computer Vision and Pattern Recognition*, 8818–8827.
- Kim, D.; Woo, S.; Lee, J.-Y.; and Kweon, I. S. 2020. Video Panoptic Segmentation. In *Proceedings of the IEEE Conference on Computer Vision and Pattern Recognition*.
- Kirillov, A.; Mintun, E.; Ravi, N.; Mao, H.; Rolland, C.; Gustafson, L.; Xiao, T.; Whitehead, S.; Berg, A. C.; Lo, W.-Y.; et al. 2023. Segment anything. *arXiv preprint arXiv:2304.02643*.
- Lee, S.; Cho, S.; and Lee, S. 2023. One-shot video inpainting. *arXiv preprint arXiv:2302.14362*.
- Lee, Y.-C.; Jang, J.-Z. G.; Chen, Y.-T.; Qiu, E.; and Huang, J.-B. 2023. Shape-aware text-driven layered video editing. In *Proceedings of the IEEE/CVF Conference on Computer Vision and Pattern Recognition*, 14317–14326.
- Li, X.; Zhang, W.; Pang, J.; Chen, K.; Cheng, G.; Tong, Y.; and Loy, C. C. 2022. Video k-net: A simple, strong, and unified baseline for video segmentation. In *CVPR*.
- Liu, Y.; Shen, C.; Yu, C.; and Wang, J. 2020. Efficient Semantic Video Segmentation with Per-frame Inference. *ECCV*.
- Liu, Y.; Zulfikar, I. E.; Luiten, J.; Dave, A.; Ramanan, D.; Leibe, B.; Ošep, A.; and Leal-Taixé, L. 2022. Opening up open world tracking. In *Proceedings of the IEEE/CVF Conference on Computer Vision and Pattern Recognition*, 19045–19055.
- Loshchilov, I.; and Hutter, F. 2017. Decoupled weight decay regularization. *arXiv preprint arXiv:1711.05101*.
- Meinhardt, T.; Feiszli, M.; Fan, Y.; Leal-Taixé, L.; and Ranjan, R. 2023. NOVIS: A Case for End-to-End Near-Online Video Instance Segmentation. *ArXiv*, abs/2308.15266.
- Miao, J.; Wang, X.; Wu, Y.; Li, W.; Zhang, X.; Wei, Y.; and Yang, Y. 2022a. Large-scale video panoptic segmentation in the wild: A benchmark. In *Proceedings of the IEEE/CVF Conference on Computer Vision and Pattern Recognition*, 21033–21043.
- Miao, J.; Wang, X.; Wu, Y.; Li, W.; Zhang, X.; Wei, Y.; and Yang, Y. 2022b. Large-Scale Video Panoptic Segmentation in the Wild: A Benchmark. In *Proceedings of the IEEE/CVF Conference on Computer Vision and Pattern Recognition (CVPR)*, 21033–21043.
- Oh, S. W.; Lee, J.-Y.; Xu, N.; and Kim, S. J. 2019. Video object segmentation using space-time memory networks. In *Proceedings of the IEEE/CVF International Conference on Computer Vision*, 9226–9235.

- Pont-Tuset, J.; Perazzi, F.; Caelles, S.; Arbeláez, P.; Sorkine-Hornung, A.; and Van Gool, L. 2017. The 2017 davis challenge on video object segmentation. *arXiv preprint arXiv:1704.00675*.
- Qi, J.; Gao, Y.; Hu, Y.; Wang, X.; Liu, X.; Bai, X.; Belongie, S.; Yuille, A.; Torr, P. H.; and Bai, S. 2022. Occluded video instance segmentation: A benchmark. *International Journal of Computer Vision*, 130(8): 2022–2039.
- Qiao, S.; Zhu, Y.; Adam, H.; Yuille, A.; and Chen, L.-C. 2020. ViP-DeepLab: Learning Visual Perception with Depth-aware Video Panoptic Segmentation. *arXiv preprint arXiv:2012.05258*.
- Rajič, F.; Ke, L.; Tai, Y.-W.; Tang, C.-K.; Danelljan, M.; and Yu, F. 2023. Segment anything meets point tracking. *arXiv* preprint arXiv:2307.01197.
- Wang, H.; Wang, W.; and Liu, J. 2021. Temporal memory attention for video semantic segmentation. In 2021 IEEE International Conference on Image Processing (ICIP), 2254–2258. IEEE.
- Wang, H.; Yan, C.; Wang, S.; Jiang, X.; Tang, X.; Hu, Y.; Xie, W.; and Gavves, E. 2023. Towards open-vocabulary video instance segmentation. In *proceedings of the IEEE/CVF international conference on computer vision*, 4057–4066.
- Wang, W.; Feiszli, M.; Wang, H.; and Tran, D. 2021. Unidentified video objects: A benchmark for dense, openworld segmentation. In *Proceedings of the IEEE/CVF International Conference on Computer Vision*, 10776–10785.
- Wu, J.; Jiang, Y.; Liu, Q.; Yuan, Z.; Bai, X.; and Bai, S. 2023. General object foundation model for images and videos at scale. *arXiv preprint arXiv:2312.09158*.
- Xu, J.; Liu, S.; Vahdat, A.; Byeon, W.; Wang, X.; and De Mello, S. 2023. Open-Vocabulary Panoptic Segmentation With Text-to-Image Diffusion Models. In *Proceedings of the IEEE/CVF Conference on Computer Vision and Pattern Recognition (CVPR)*, 2955–2966.
- Xu, N.; Yang, L.; Fan, Y.; Yue, D.; Liang, Y.; Yang, J.; and Huang, T. 2018. Youtube-vos: A large-scale video object segmentation benchmark. *arXiv preprint arXiv:1809.03327*.
- Xue, H.; Hang, T.; Zeng, Y.; Sun, Y.; Liu, B.; Yang, H.; Fu, J.; and Guo, B. 2022. Advancing High-Resolution Video-Language Representation with Large-Scale Video Transcriptions. In *International Conference on Computer Vision and Pattern Recognition (CVPR)*.
- Yang, L.; Fan, Y.; and Xu, N. 2019. Video instance segmentation. In *Proceedings of the IEEE/CVF International Conference on Computer Vision*, 5188–5197.
- Yang, Z.; Wei, Y.; and Yang, Y. 2021. Associating objects with transformers for video object segmentation. *Advances in Neural Information Processing Systems*, 34: 2491–2502.
- Zhang, R.; Jiang, Z.; Guo, Z.; Yan, S.; Pan, J.; Ma, X.; Dong, H.; Gao, P.; and Li, H. 2023a. Personalize segment anything model with one shot. *arXiv preprint arXiv:2305.03048*.
- Zhang, T.; Tian, X.; Zhou, Y.; Ji, S.; Wang, X.; Tao, X.; Zhang, Y.; Wan, P.; Wang, Z.; and Wu, Y. 2023b. DVIS++: Improved Decoupled Framework for Universal Video Segmentation. arXiv:2312.13305.

Zhang, Z.; Wu, B.; Wang, X.; Luo, Y.; Zhang, L.; Zhao, Y.; Vajda, P.; Metaxas, D.; and Yu, L. 2024. AVID: Any-Length Video Inpainting with Diffusion Model. In *Proceedings of the IEEE/CVF Conference on Computer Vision and Pattern Recognition*, 7162–7172.

Zhou, T.; Luo, W.; Ye, Q.; Shi, Z.; and Chen, J. 2024. SAM-PD: How Far Can SAM Take Us in Tracking and Segmenting Anything in Videos by Prompt Denoising. *arXiv* preprint *arXiv*:2403.04194.

Zhu, J.; Chen, Z.; Hao, Z.; Chang, S.; Zhang, L.; Wang, D.; Lu, H.; Luo, B.; He, J.-Y.; Lan, J.-P.; et al. 2023. Tracking anything in high quality. *arXiv* preprint arXiv:2307.13974.

Zulfikar, I. E.; Mahadevan, S.; Voigtlaender, P.; and Leibe, B. 2024. Point-VOS: Pointing Up Video Object Segmentation. *arXiv preprint arXiv:2402.05917*.

Appendix

The following sections present more examination of our results, including a detailed explanation of our methodology, as well as supplementary visualizations of our MUG-VOS and MMPM results. Section A provide details of data collection pipeline, including annotation tools for constructing video segmentation dataset. Section B delves into the specific implementation details of our method, including used losses, hyper-parameter settings, and data augmentations implemented on our training methods. Section C provides additional experiments comparing the performance of MMPM with previous methods. Section D highlights the quality of our MUG-VOS dataset. Our MUG-VOS dataset not only features a higher density of masks but also maintains high-quality annotations. Furthermore, MUG-VOS includes a diverse range of multi-granularity masks, setting it apart from other existing benchmarks. Section E provides additional qualitative results on MUG-VOS test set.

A. Details of data collection pipeline

We provide detailed algorithm of MUG-VOS data collection pipeline. See Algorithm 1 for specific details.

Algorithm 1: Data Collection Pipeline Algorithm

```
Require: Video V = \{v_t | t \in [1, T]\}, initial frame v_1, SAM
     model, flow model
 1: for t = 1 to T do
        Obtain foreground masks M_t^i for frame v_t
 2:
 3:
        if t > 1 then
           Sample points \hat{P}_t^i from M_{t-1}^i in random
 4:
           Get warped points P_t^i = \text{warp}(\hat{P}_t^i, F_{t-1 \to t})
 5:
           Predict candidate masks \hat{M}_t^i = \text{SAM}(v_t, P_t^i)
 6:
           Get warped mask \tilde{M}_{t-1}^i = \operatorname{warp}(M_{t-1}^i, F_{t-1 \to t})
 7:
           Compute IoU between \tilde{M}_{t-1}^i and \hat{M}_t^i
 8:
           Select M_t^i = \arg\max_{\hat{M}_t^i} \text{IoU}(\tilde{M}_{t-1}^i, \hat{M}_t^i)
 9:
10:
           Initialize M_1^i using SAM with grid point prompts
11:
        end if
12:
13: end for
```

We also developed specialized annotation tools to enhance the efficiency of our workflow, as shown in Fig. 5. Initially, supervisors select multi-granularity masks from the first frame, which include categories such as "stuff", "thing", or "non-salient objects" that need to be tracked, using SAM (Segment Anything Model) (Kirillov et al. 2023). Annotators then verify whether the masks generated by the data collection pipeline are consistent with those from the first and previous frames. If the masks are inconsistent, annotators refine the masks by prompting points to SAM. Once a mask track is complete, the results are reviewed by supervisors to ensure the track is both consistent and smooth.

As SAM provides stability and IoU prediction scores, annotators can use these scores to ensure they generated the fine-grained masks. Additionally, besides picking foreground points during the refine process, annotators can also select negative points to obtain the desired masks.

B. Implementation details

B.1 Architecture

We employ MMPM, which leverages the SAM image encoder pretrained on the SA-1B dataset. The pretrained SAM encoder, based on the Vision Transformer architecture, is initialized with 'image segment anything' weights. We use SAM-Base as our visual encoder. Additionally, we introduce a memory architecture comprising two types of memory. These memory types enhance image features by utilizing previous results, enabling the model to effectively segment multi-granularity objects by integrating information from previous frames with current image details.

To efficiently combine information from multiple frames, we implemented an affinity matrix based on a similarity matrix. The similarity matrix is calculated by comparing key elements with the query element, using the same similarity calculation method as in STCN (Cheng, Tai, and Tang 2021) and XMem (Cheng and Schwing 2022). The affinity matrix is then obtained by applying the softmax function to the similarity matrix.

B.2 Training details

In this subsection, we detail the training procedures for MMPM, XMem, and DEVA. To ensure a fair comparison, we trained XMem and DEVA on the MUG-VOS training set alongside MMPM. For MMPM training, we divided the process into two stages. First, we trained MMPM on a static image dataset, applying independent augmentations to simulate video-like sequences. This step helps the model learn to handle static images as if they were part of a video. In the second stage, we trained MMPM on the MUG-VOS training set. We used the AdamW (Loshchilov and Hutter 2017) optimizer with a learning rate of 1e-5. The model was trained for 200K iterations with a batch size of 3, followed by 250K iterations with a batch size of 4.

To input an image into the SAM encoder, we selected the longest axis of the image and resized it to 1024 pixels, scaling the other axis proportionally to maintain the original aspect ratio. To increase the complexity during training, we augmented the MUG-VOS dataset with random cropping, horizontal flipping, and affine transformations. Additionally, given that we are working with a video dataset, we randomly shuffled the image order to improve the model's learning of video sequences.

For XMem and DEVA, we used the same dataset that was employed for MMPM training, adhering to the training procedures outlined in their respective papers. Specifically, we trained DEVA on a static image dataset with a batch size of 32 for 40K iterations. For XMem, we utilized the stage 0 model provided by the original repository.

After training on the static dataset, we directly trained both models on the MUG-VOS training set. XMem was trained for an additional 11K iterations with batch size 16, while the DEVA model was trained for 7.5K iterations with batch size 16.

DAVIS-2017	$\mathcal{J}\&\mathcal{F}$	\mathcal{J}	\mathcal{F}
XMem (Cheng and Schwing 2022)	63.0	59.7	66.4
DEVA (Cheng et al. 2023)	64.1	60.8	67.4
MMPM	<u>69.1</u>	<u>66.0</u>	<u>72.1</u>

Table A.1: The quantitative evaluation of video object segmentation on DAVIS-2017 (Pont-Tuset et al. 2017) validation set. Note that all the models are trained on the MUG-VOS train set.

C. Experimental results

We evaluated our method on the DAVIS-2017 (Pont-Tuset et al. 2017) dataset. To ensure a fair comparison, all trainable methods listed in Table 2, including MMPM, were trained uniformly on the MUG-VOS Train set and utilized the same mask prompt to standardize input and output formats. Furthermore, DEVA, XMem, and MMPM were exclusively trained on the MUG-VOS Train set and subsequently evaluated on DAVIS-2017. Our results are presented in Table A.1.

D. MUG-VOS visualization

We present the qualitative results of the MUG-VOS test dataset, which includes 0.663 density, 59k masks, 887 mask tracks, 29.6 masks per frame, and 1,999 annotated frames, as shown from Fig. A.2 to Fig. A.3. Additionally, we provide a qualitative comparison between the ground truth masks of existing benchmarks and the masks generated by our data collection pipeline, illustrated from Fig. A.4 to Fig.A.6. Our data collection pipeline allows us to construct a dataset annotated with masks of more varied granularity than those found in existing benchmarks. Further visualizations of the MUG-VOS dataset, organized by the number of mask tracks, are presented from Fig. A.7 to Fig. A.8.

E. Additional qualitative results

We provide additional qualitative results of MMPM on our proposed MUG-VOS dataset from Fig.A.9 to Fig.A.10. Our MMPM demonstrates superior results compared to other methods. As shown in the figures, other methods, except for MMPM, either made tracking errors or generated unstable masks. However, MMPM confidently produced fine-grained segmentation masks, highlighting its ability to accurately track and segment multi-granularity objects.

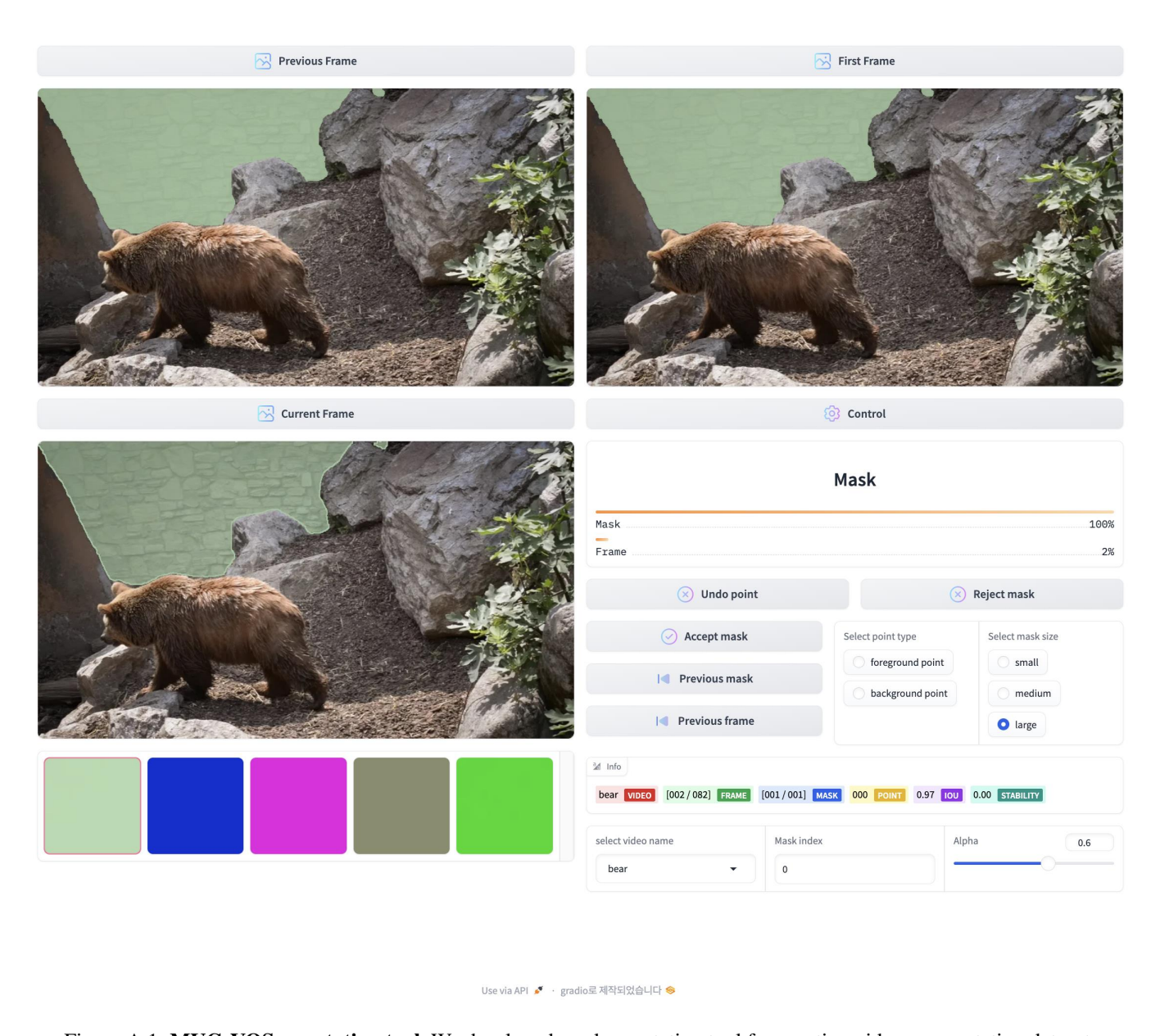


Figure A.1: MUG-VOS annotation tool. We developed mask annotation tool for curating video segmentation dataset.



Figure A.2: **MUG-VOS test dataset.** To mitigate the accumulation of errors within the automated process, annotators were directed to either approve or reject the mask tracks generated by the data collection pipeline. In instances where errors were detected, the annotators performed frame-level refinements of the masks utilizing the Segment Anything Model.



Figure A.3: **MUG-VOS test dataset.** To mitigate the accumulation of errors within the automated process, annotators were directed to either approve or reject the mask tracks generated by the data collection pipeline. In instances where errors were detected, the annotators performed frame-level refinements of the masks utilizing the Segment Anything Model.

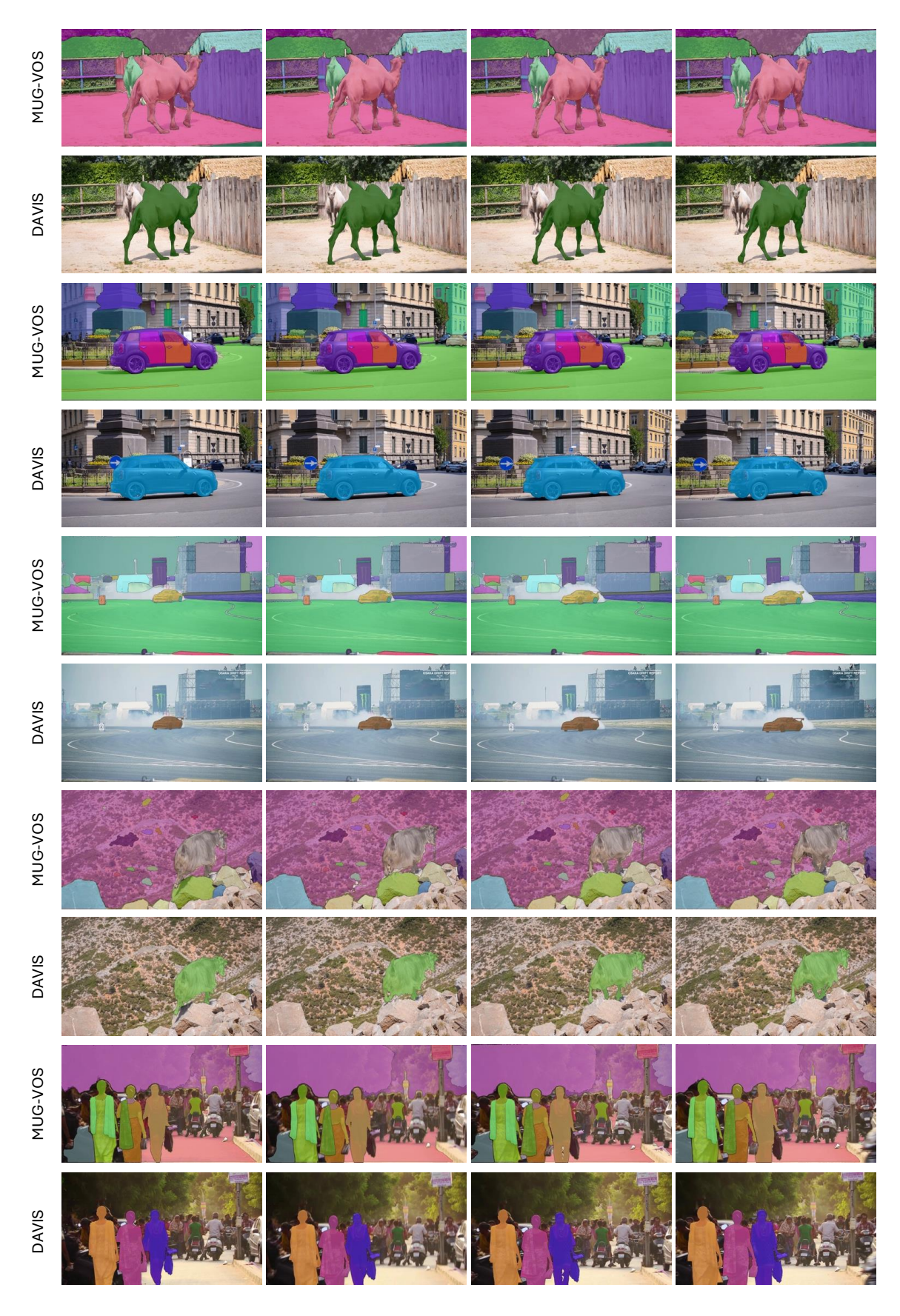


Figure A.4: **Mask comparison.** We qualitatively compare mask generation quality of **our data collection pipeline** with ground-truth from DAVIS (Pont-Tuset et al. 2017), Youtube-VOS (Xu et al. 2018), and UVO (Wang et al. 2021).

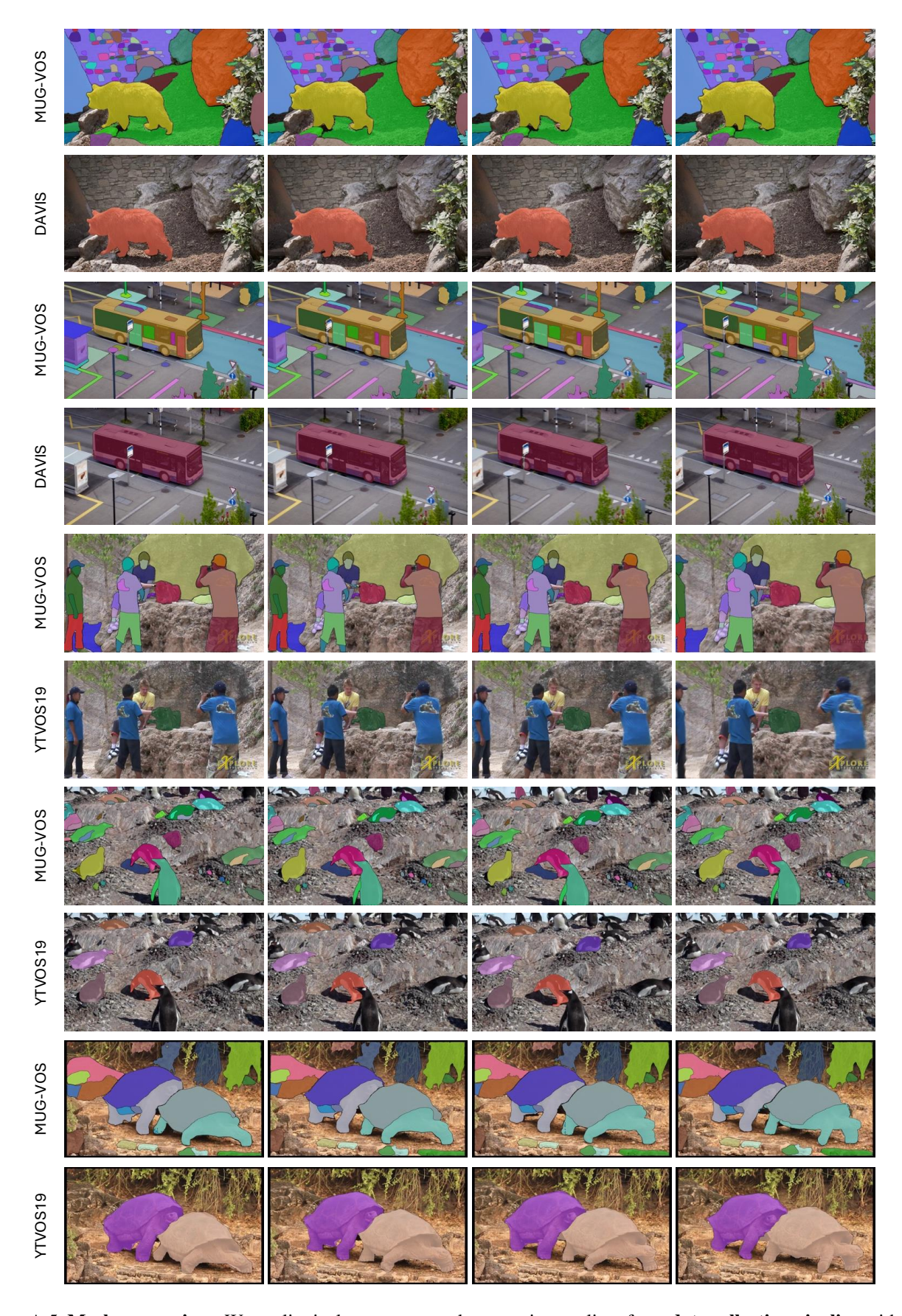


Figure A.5: **Mask comparison.** We qualitatively compare mask generation quality of **our data collection pipeline** with ground-truth from DAVIS (Pont-Tuset et al. 2017), Youtube-VOS (Xu et al. 2018), and UVO (Wang et al. 2021).

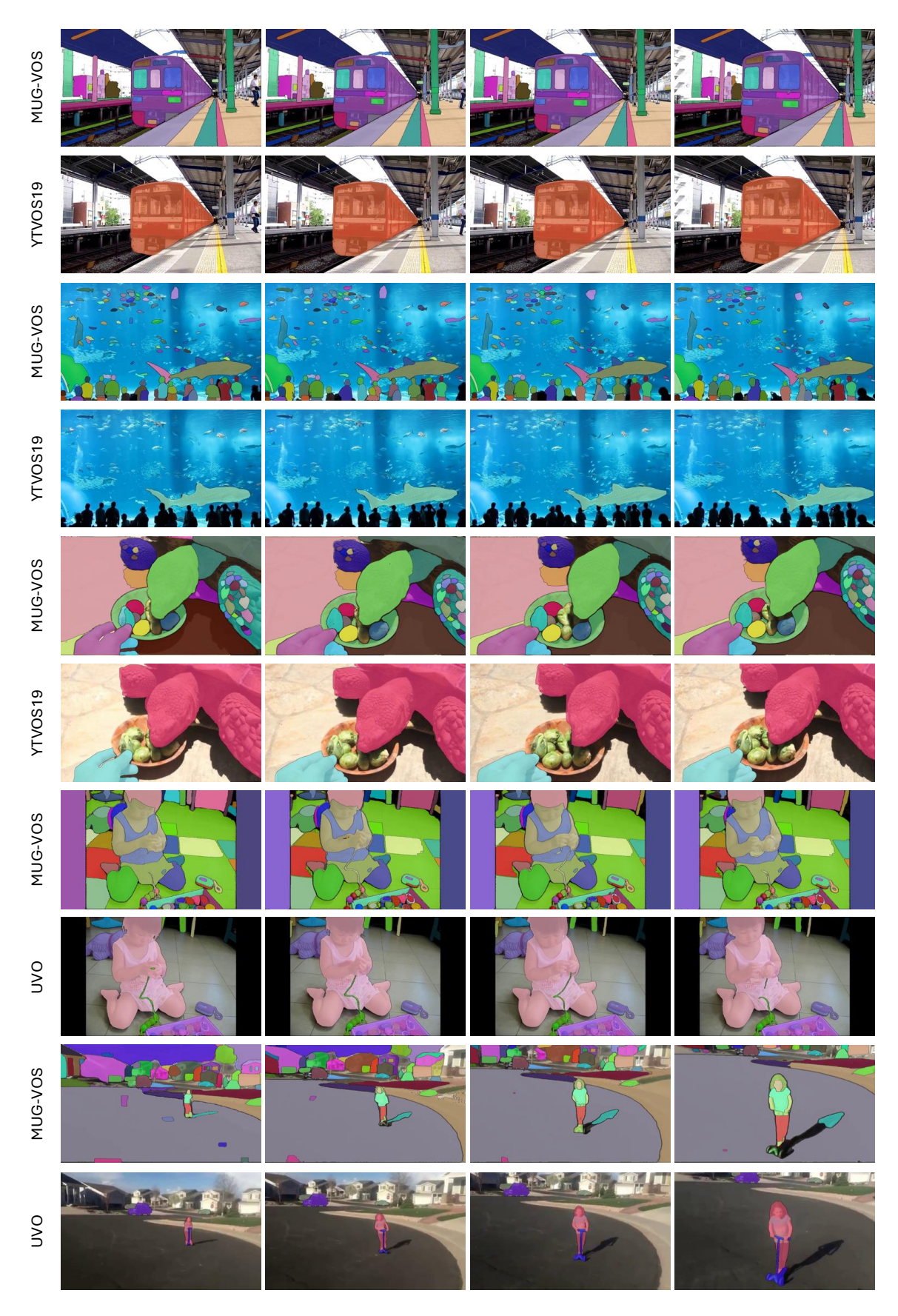


Figure A.6: **Mask comparison.** We qualitatively compare mask generation quality of **our data collection pipeline** with ground-truth from DAVIS (Pont-Tuset et al. 2017), Youtube-VOS (Xu et al. 2018), and UVO (Wang et al. 2021).

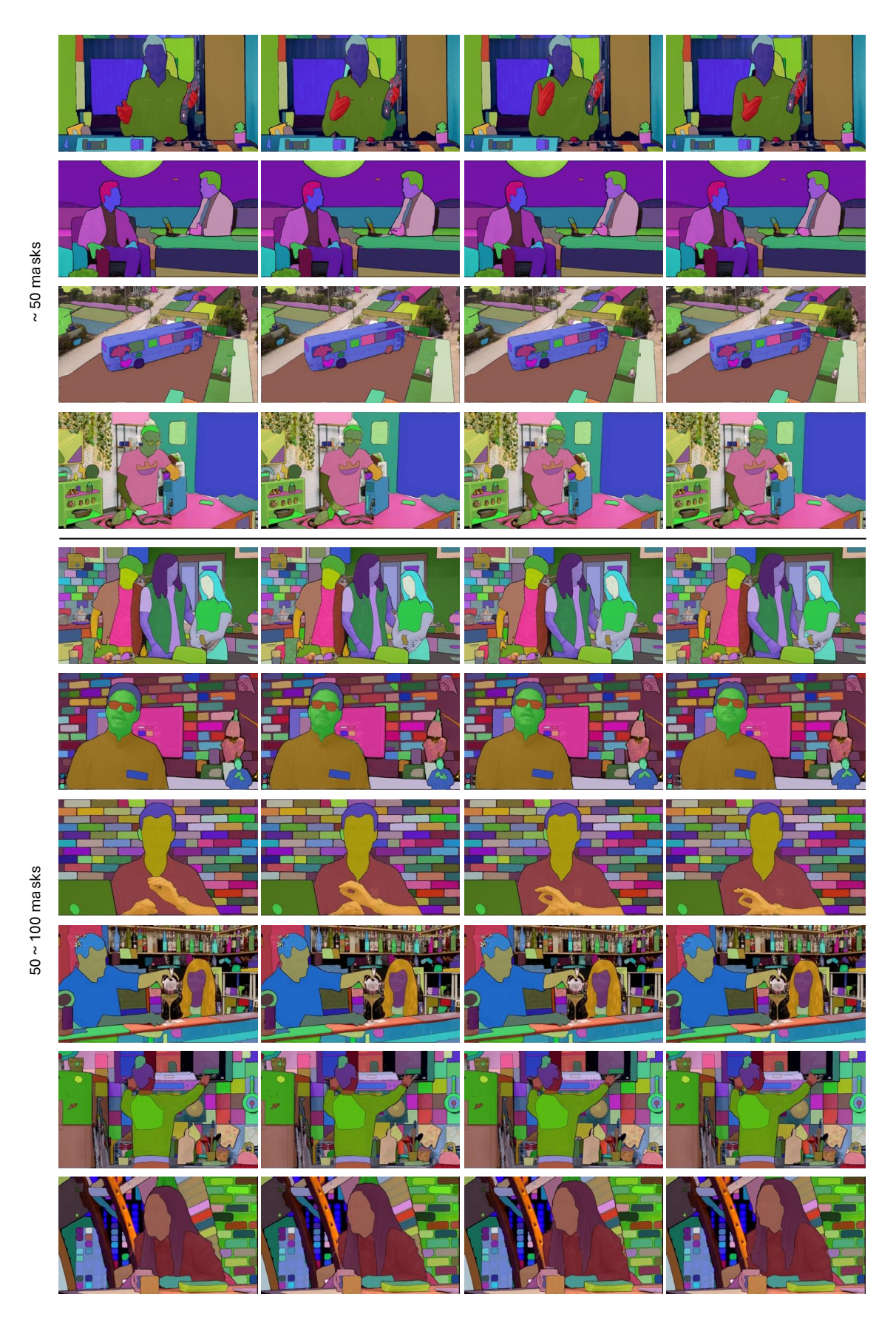


Figure A.7: **Example image sequences with overlaid masks from our MUG-VOS dataset.** These masks are generated by our data collection pipeline *fully automatically*. We group videos by number of masks per frame for visualization.

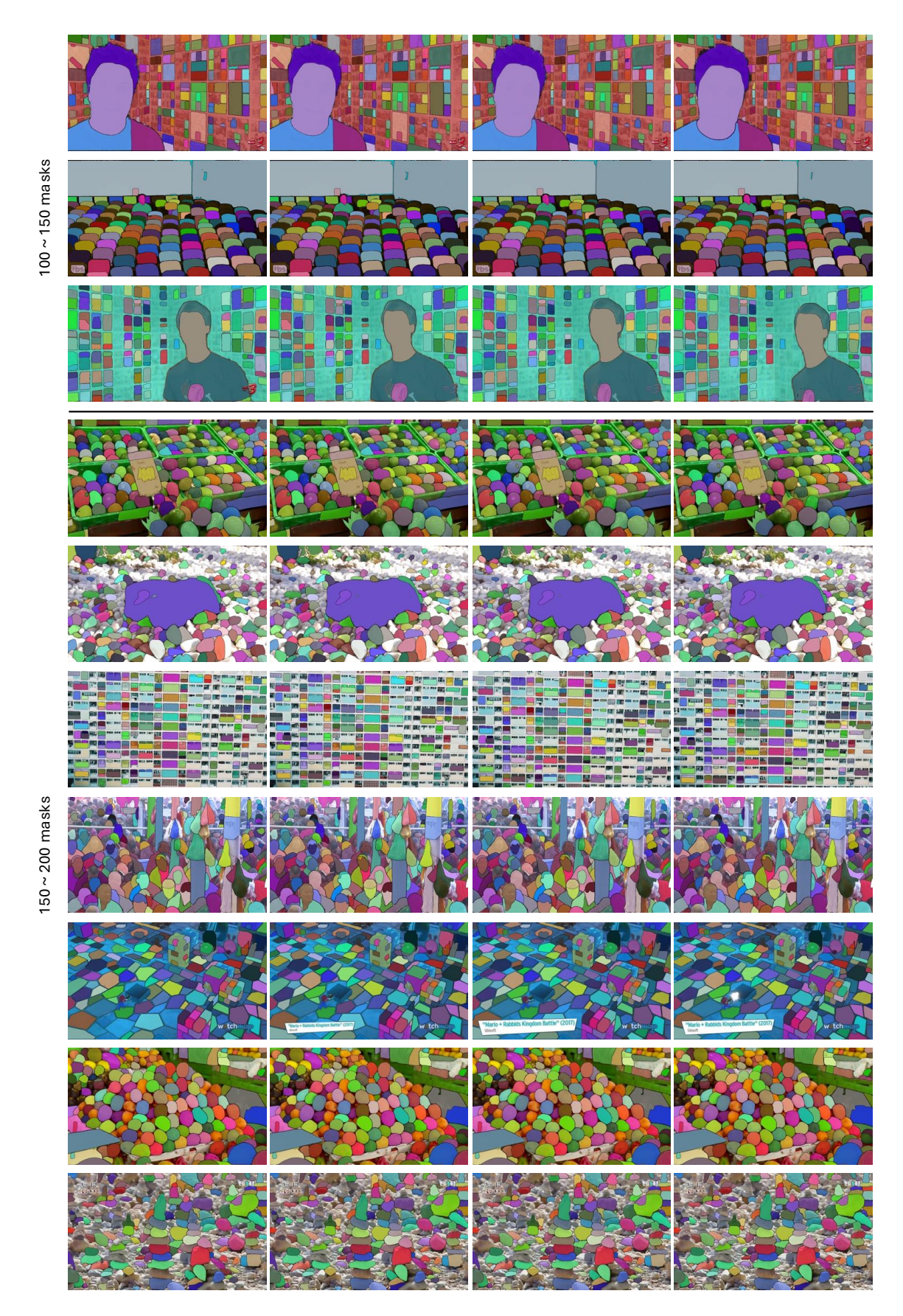


Figure A.8: **Example image sequences with overlaid masks from our MUG-VOS dataset.** These masks are generated by our data collection pipeline *fully automatically*. We group videos by number of masks per frame for visualization.



Figure A.9: **Qualitative comparison.** We qualitatively compare mask generation quality of **our data collection pipeline** with ground-truth from DAVIS (Pont-Tuset et al. 2017), Youtube-VOS (Xu et al. 2018), and UVO (Wang et al. 2021).



Figure A.10: **Qualitative comparison.** We qualitatively compare mask generation quality of **our data collection pipeline** with ground-truth from DAVIS (Pont-Tuset et al. 2017), Youtube-VOS (Xu et al. 2018), and UVO (Wang et al. 2021).